Full-Wave Analysis of Coplanar Waveguide and Slotline Using the Time-Domain Finite-Difference Method

GUO-CHUN LIANG, STUDENT MEMBER, IEEE, YAO-WU LIU, AND KENNETH K. MEI, FELLOW, IEEE

Abstract—**We have presented a detailed full-wave analysis of a coplanar waveguide (CPW) and a slotline by the time-domain finite-difference method (TD–FD). The transient propagating waveforms along the coplanar waveguide and slotline, which are excited by retarded Gaussian pulses, are found in the time domain. After the time-domain field distributions are obtained, frequency-domain parameters such as the effective dielectric constant and the complex characteristic impedance are calculated using Fourier transformations. The results agree well with available theoretical and experimental data over a wide frequency range. We have also checked the validity of the quasi-TEM assumptions for CPW and slotline analyses. This is done by evaluating the ratios of the longitudinal and transverse field components directly.**

I. Introduction

COPLANAR waveguides and slotlines are important planar transmission lines in microwave and millimeter-wave integrated circuits. Analysis methods are presently available in the frequency domain [1]–[3].

In this paper, we present a full-wave analysis of the CPW and slotline in the time domain. The analysis offers several important benefits: all modes are taken into consideration simultaneously and no assumptions other than equation discretization and mesh termination are made. In addition, information including radiation effects for the entire frequency range of interest can be obtained from a single calculation; visualization of wave dispersion is a by-product of the computation. The method is applicable, for example, to microstrip lines [4], coplanar strips, slotlines [5], and coplanar waveguides [6].

The TD–FD method begins with finding the transient propagating waveforms along the coplanar waveguide by solving Maxwell's equations directly, followed by the evaluation of parameters that characterize the transmission line. Since the time-domain method provides a detailed solution everywhere in the computation domain, we can check the validity of the quasi-TEM assumption for the CPW and slotline analyses by evaluating the longitudinal and transverse field components. The main issues are presented and discussed in the following sections.

Manuscript received March 31, 1989; revised July 14, 1989. This work was supported in part by the Joint Services Electronics Program under Contract F49620-87-C-0041 and by the Microelectronics Innovation and Computer Research Opportunities program under Proposal 88-111.

The authors are with the Department of Electrical Engineering and Computer Sciences, University of California, Berkeley, CA 94720.

IEEE Log Number 8930943.

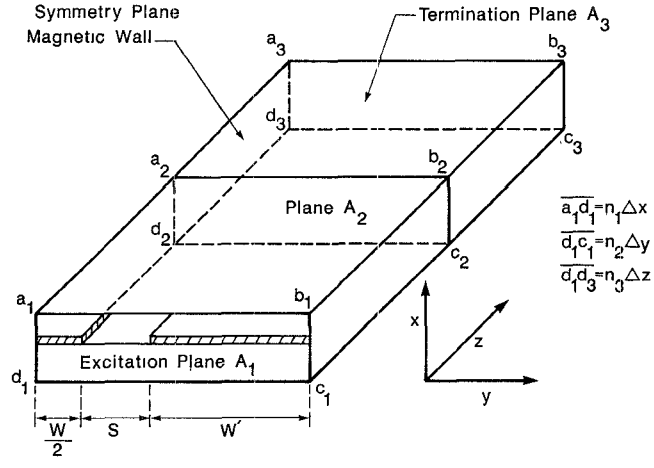

Fig. 1. Schematic diagram for computation domain and boundary condition treatment. $A_1(a_1b_1c_1d_1)$ is an excitation plane and $A_3(a_3b_3c_3d_3)$ is a termination plane. The symmetry plane $(a_1a_3d_3d_1)$ is replaced by a magnetic wall for CPW and an electrical wall for slotline.

II. Pulse Excitation

A retarded Gaussian pulse is usually used as an excitation in time-domain calculation due to its smoothness in time, and the ease with which it can be adjusted for a specific pulse width. It is also the easiest excitation for boundary condition treatment.

Care is taken in the formulation of the spatial distributions on the excitation plane (plane A_1 in Fig. 1). The quasi-static, approximated field distributions are exploited as an initial distribution for both the CPW and the slotline. The choice of the spatial distributions directly affects the boundary treatment and the time taken to reach a stable field distribution. The complete excitation pulse at time step $t = t_n$ can be expressed as

$$E_x(x, y, t_n) = \Psi_x(x, y)\exp\left[-\frac{(t_n - t_0)^2}{T^2}\right] \quad (1)$$

$$E_y(x, y, t_n) = \Psi_y(x, y)\exp\left[-\frac{(t_n - t_0)^2}{T^2}\right] \quad (2)$$

0018-9480/89/1200-1949$01.00 ©1989 IEEE

where $\Psi_x(x, y)$ and $\Psi_y(x, y)$ are the previously mentioned spatial distributions. They are different for CPW and slotline, and t_0 is chosen to ensure the causality of the problem and to keep the discontinuity at $t = 0$ very small. It is observed that the different choices of spatial distributions will only affect the time it takes to reach a stable field distribution on the line, not the distribution itself.

III. Boundary Truncation

Coplanar waveguides and slotlines are both open structures; therefore artificial boundaries must be employed to truncate the mesh. Referring to Fig. 1, plane A_1 ($a_1b_1c_1d_1$) is the excitation plane, and the fields $E_x(x, y, t)$ and $E_y(x, y, t)$ on this plane are specified according to (1) and (2). The plane of symmetry ($a_3a_1d_1d_3$) is replaced by a magnetic wall for CPW and an electric wall for slotline, so that only half the region need be considered. The other four boundary planes have to be replaced by a set of artificial "absorbing boundary walls." We should minimize the reflection from those artificial walls since Fourier transforms are very sensitive to errors caused by reflected waves from the boundaries. This is one of the reasons why the time-domain method is frequently used to obtain qualitative results, rather than to obtain frequency-dependent parameters or design data.

Due to the geometry of the CPW and slotline structures, the boundary treatment is more complex than that of microstrip line [4]. The field lines are localized mainly between the two plates for microstrips, and the "exact" boundary conditions can be applied to the bottom plane ($E_t = 0$, $H_n = 0$). But for coplanar waveguides and slotlines, no "exact" boundary conditions can be used. The fields are quite spread out in space, especially for lines with low-permittivity substrates. Furthermore, the absorbing boundary walls on the sides (plane $b_1b_3c_3c_1$) have a metal sheet sandwiched between two media with different propagation velocities. In order to treat this special case, the field components at points near the boundary are obtained by a proper weighting of the field values found using two different methods. The field at step t_n is $\vec{E}_i^{(n)} = c_1\vec{E}_{1i}^{(n)} + c_2\vec{E}_{2i}^{(n)}$, where c_1 and c_2 are coefficients to be determined. $\vec{E}_{1i}^{(n)}$ is obtained by Mur's absorbing boundary formula [7]; the other $\vec{E}_{2i}^{(n)}$ is computed from the fields at surrounding points, a half time step earlier by the discretized Maxwell's equations [8]. The procedures to deal with $\vec{H}$ fields are similar. This method is based on reflection error cancellations and is discussed in [9] for a two-dimensional uniform medium case.

In the simulation, we need to treat the air–dielectric interface for both the CPW and the slotline. The formulation on the interface can be made explicitly. Let us consider a general case. Imagine an interface plane perpendicular to the x axis. The upper medium has conductivity σ^+ and permittivity ϵ^+, and the lower medium σ^- and ϵ^-. Start with Maxwell's equation:

$$\nabla \times \vec{H} = \sigma\vec{E} + \epsilon\frac{\partial \vec{E}}{\partial t} \tag{3}$$

where σ and ϵ take on their respective values in each medium. We can obtain continuity equations across the interface as follows:

$$\frac{\sigma^+ + \sigma^-}{2}E_z + \frac{\epsilon^+ + \epsilon^-}{2}\frac{\partial E_z}{\partial t} = \frac{\Delta H_y}{\Delta x} - \frac{\partial H_x}{\partial y} \tag{4}$$

with

$$\frac{\Delta H_y}{\Delta x} = \frac{H_y(i+1, j, k) - H_y(i-1, j, k)}{\Delta x} \tag{5}$$

and

$$\frac{\sigma^+ + \sigma^-}{2}E_y + \frac{\epsilon^+ + \epsilon^-}{2}\frac{\partial E_y}{\partial t} = \frac{\partial H_x}{\partial z} - \frac{\Delta H_z}{\Delta x} \tag{6}$$

with

$$\frac{\Delta H_z}{\Delta x} = \frac{H_z(i+1, j, k) - H_z(i-1, j, k)}{\Delta x}. \tag{7}$$

Equations (4) and (6) can be understood physically as involving the simple average of the parameters of the two media.

IV. Field Calculations

After setting up the simulation domain and subsequent pulse excitation, we can evaluate the field distributions produced by the given Gaussian pulse over the whole computation region. The fields are governed by Maxwell's equations. For our geometry, Yee's mesh is used to accommodate the details of the structure [8]. The arrangement of the grid greatly simplifies the discretized difference equations, which can be written as follows:

$$B_x^{n+\frac{1}{2}}(i, j, k) = B_x^{n-\frac{1}{2}}(i, j, k) - \Delta t\left[\frac{E_z^n(i, j, k) - E_z^n(i, j-1, k)}{\Delta y} - \frac{E_y^n(i, j, k) - E_y^n(i, j, k-1)}{\Delta z}\right] \tag{8}$$

$$B_y^{n+\frac{1}{2}}(i, j, k) = B_y^{n-\frac{1}{2}}(i, j, k) - \Delta t\left[\frac{E_x^n(i, j, k) - E_x^n(i, j, k-1)}{\Delta z} - \frac{E_z^n(i, j, k) - E_z^n(i-1, j, k)}{\Delta x}\right] \tag{9}$$

$$B_z^{n+\frac{1}{2}}(i, j, k) = B_z^{n-\frac{1}{2}}(i, j, k) - \Delta t\left[\frac{E_y^n(i, j, k) - E_y^n(i-1, j, k)}{\Delta x} - \frac{E_x^n(i, j, k) - E_x^n(i, j-1, k)}{\Delta y}\right] \tag{10}$$

$$D_x^{n+1}(i,j,k) = D_x^n(i,j,k) + \Delta t\left[\frac{H_z^{n+\frac{1}{2}}(i,j+1,k) - H_z^{n+\frac{1}{2}}(i,j,k)}{\Delta y} - \frac{H_y^{n+\frac{1}{2}}(i,j,k+1) - H_y^{n+\frac{1}{2}}(i,j,k)}{\Delta z}\right] \quad (11)$$

$$D_y^{n+1}(i,j,k) = D_y^n(i,j,k) + \Delta t\left[\frac{H_x^{n+\frac{1}{2}}(i,j,k+1) - H_x^{n+\frac{1}{2}}(i,j,k)}{\Delta z} - \frac{H_z^{n+\frac{1}{2}}(i+1,j,k) - H_z^{n+\frac{1}{2}}(i,j,k)}{\Delta x}\right] \quad (12)$$

$$D_z^{n+1}(i,j,k) = D_z^n(i,j,k) + \Delta t\left[\frac{H_y^{n+\frac{1}{2}}(i+1,j,k) - H_y^{n+\frac{1}{2}}(i,j,k)}{\Delta x} - \frac{H_x^{n+\frac{1}{2}}(i,j+1,k) - H_x^{n+\frac{1}{2}}(i,j,k)}{\Delta y}\right]. \quad (13)$$

For general anisotropic media, the expressions for $\vec{H}$ and $\vec{E}$ are

$$\vec{H} = \overleftrightarrow{\mu}^{-1}\vec{B} \quad (14)$$

$$\vec{E} = \overleftrightarrow{\epsilon}^{-1}\vec{D}. \quad (15)$$

Starting from the initial fields, we can find the magnetic field $\vec{B}$ from (8)–(10) and $\vec{H}$ from (14). Similarly, the displacement vector $\vec{D}$ can be found using (11)–(13), and the electric field $\vec{E}$ from (15). For isotropic media, only (8) through (13) are needed, substituting $\vec{H}$ for $\vec{B}$, $\vec{E}$ for $\vec{D}$, and $\Delta t/\mu$ for Δt in (8)–(10) and $\Delta t/\epsilon$ for Δt in (11)–(13). In summary, starting from the proper initial fields, we can find the electric and magnetic fields within the computation domain at alternate half-time steps according to the discretized Maxwell's equations.

V. Parameter Evaluation

After finding the field distribution in the time domain, we may find the frequency-domain parameters by the Fourier transform. Let the waveforms on the transmission line be $w(t,z_i)$ and $w(t,z_j)$ at $z=z_i$ and $z=z_j$, respectively, where $w(t,z)$ can be either the electric or the magnetic field. The following relation holds for the segment $\overline{z_iz_j}$:

$$F\left[w(t,z_j)\right] = F\left[w(t,z_i)\right]e^{-\gamma(\omega,\overline{z_iz_j})(z_j-z_i)} \quad (16a)$$

where $F[\cdots]$ denotes the Fourier transformation operator. Equation (16a) can be used to evaluate the propagation constant γ:

$$\gamma\left(\omega,\overline{z_iz_j}\right) = \frac{1}{z_j-z_i}\ln\left\{\frac{F\left[w(t,z_i)\right]}{F\left[w(t,z_j)\right]}\right\}. \quad (16b)$$

Furthermore, we can define the effective dielectric constant as

$$\epsilon_{\text{eff}}(\omega) \triangleq \frac{\beta^2(\omega)}{\omega^2\mu_o}. \quad (17)$$

Ideally, the propagation constant $\gamma(\omega,\overline{z_iz_j}) = \alpha(\omega,\overline{z_iz_j}) + j\beta(\omega,\overline{z_iz_j})$ for the segment $\overline{z_iz_j}$ should be independent of positions z_i and z_j. In reality, $\gamma(\omega)$ obtained from different segments will not be the same, because of the errors caused by the imperfect boundary treatment. Notice that $\Delta z = z_j - z_i$ should not be made too small; otherwise γ will not be accurate due to numerical error. A typical Δz is 10 to 15 spatial steps. The noise due to the imperfect boundary treatment can be reduced by averaging the γ's obtained from different segments $\overline{z_iz_j}$ or by using the least-squares method since part of the noise is random noise.

Another important parameter is the characteristic impedance $Z(\omega)$. This impedance cannot be defined uniquely for CPW's and slotlines, because the modes on the line are non-TEM. In this study, a voltage–current definition is employed for simplicity. The impedance evaluated at $z=z_i$ can be defined as

$$Z(\omega,z_i) \triangleq \frac{F\left[V(t,z_i)\right]}{F\left[I(t,z_i)\right]} \quad (18)$$

where $V(t,z_i)$ is the voltage and $I(t,z_i)$ is the current, both evaluated at $z=z_i$. The current $V(t,z_i)$ and $I(t,z_i)$ are defined as follows:

$$V(t,z_i) \triangleq \int_a^b \vec{E}(x,y,t,z_i)\cdot d\vec{\xi} \quad (19)$$

$$I(t,z_i) \triangleq \oint_c \vec{H}(x,y,t,z_i)\cdot d\vec{l} \quad (20)$$

where, for the coplanar waveguide, point a is on the center strip, and b is on the side strip. The integration loop c encloses the center strip. For the slotline, on the other hand, points a and b are on the two side strips, and loop c encloses either of the strips (actually, part of the loop is on the absorbing boundary). Integrations have been carried out with different paths and loops, showing that differences between impedance for various paths are negligible as long as H_z and E_z are not too large.

TABLE I

Parameters for CPW	Case 1	Case 2
Center strip width W (mm)	0.135	0.4
Strip spacing S (mm)	0.065	0.5
Side strip width W′ (mm)	0.59	infinite
Substrate thickness H (mm)	0.5	1.0
Metal strip thickness T (mm)	0.0	0.0
Space step *dh* (mm)	0.0135	0.050
Time step *dt* (ps)	0.0176	0.0858
Relative dielectric constant ε_r	12.9	20.0

Thus far in the simulation, the transmission line has been terminated by a matched impedance. Equivalently, the absorbing condition is applied at the four boundary planes as indicated in Fig. 1. We can also obtain results for $\gamma(\omega)$ and $Z(\omega)$ by a combination of electric (shorted end) and magnetic (open-ended) wall terminations, while keeping the other three planes absorbing. In other words, we simulate the problem twice, first by applying the electric wall at plane A_3 ($a_3b_3c_3d_3$), and then the magnetic wall at the same plane, keeping the other three planes absorbing. From the basic transmission line equations, we can directly obtain expressions for the propagation constant and the characteristic impedance as follows:

$$\gamma(\omega, z_i) = \frac{1}{2z_i} \ln \left[\frac{\sqrt{\left(\frac{V(\omega, z_i)}{I(\omega, z_i)} \right)_o} + \sqrt{\left(\frac{V(\omega, z_i)}{I(\omega, z_i)} \right)_s}}{\sqrt{\left(\frac{V(\omega, z_i)}{I(\omega, z_i)} \right)_o} - \sqrt{\left(\frac{V(\omega, z_i)}{I(\omega, z_i)} \right)_s}} \right] \tag{21}$$

$$Z(\omega, z_i) = \sqrt{\left(\frac{V(\omega, z_i)}{I(\omega, z_i)} \right)_o \cdot \left(\frac{V(\omega, z_i)}{I(\omega, z_i)} \right)_s} \tag{22}$$

where $\gamma(\omega, z_i)$ and $Z(\omega, z_i)$ are found at $z = z_i$. The subscripts s and o represent shorted and open terminations, respectively.

VI. Numerical Implementation

A. Calculation Setup

For coplanar waveguides, we have analyzed two cases (cases 1 and 2). Their geometric and computation parameters are summarized in Table I.

For slotline, the thickness of the substrate is $H = 0.1$ mm, and the slot width $W = 0.06$ mm. The thickness of the metal strip is assumed to be zero and the width of the substrate B is assumed to be infinite (see Fig. 3(b)), for simplicity. Space step *dh* and time step *dt* are chosen as 10 μm and 0.017 ps, respectively.

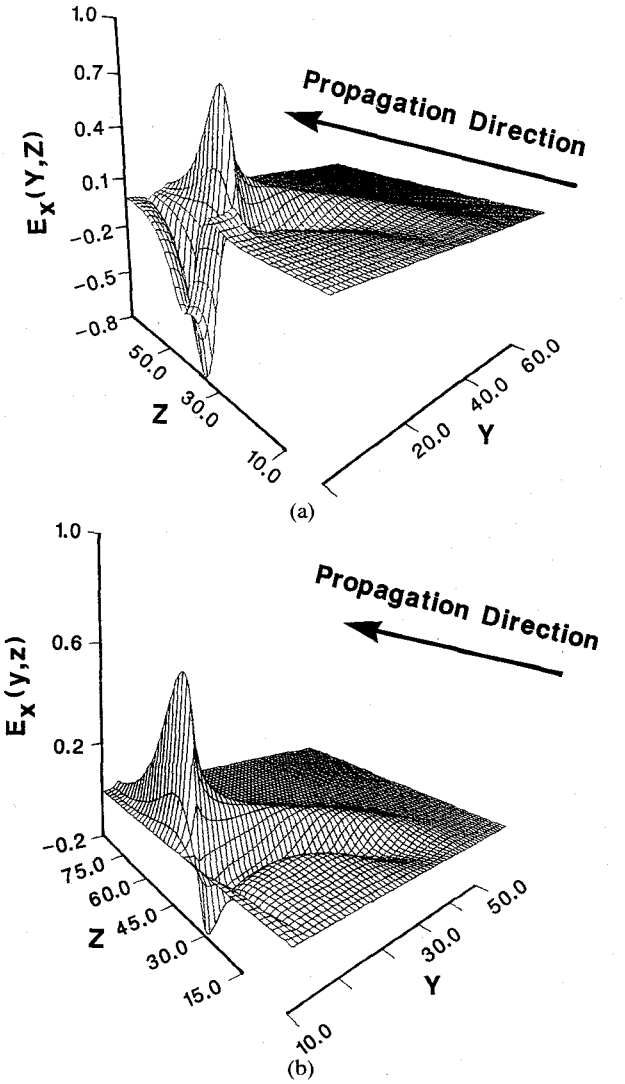

Fig. 2. (a) The spatial waveforms of the E_x component for the CPW (case 1), which is sampled just below the strips. Edge effect and surface wave excitation are clearly illustrated in the figure. (b) The spatial waveforms of the E_x component for slotline, which is also sampled just below the strips.

The computation domain is a box with sides $(n_1\Delta x)\times(n_2\Delta y)\times(n_3\Delta z)$, which is usually determined by the available memory. For the current calculation, n_1, n_2, and n_3 are 55, 60, and 100, respectively. The computation spatial step *dh* is chosen to accommodate the structures conveniently, and the time step *dt* is selected to satisfy the stability conditions.

B. Spatial Field Distribution and Waveforms of the Field Components

Fig. 2(a) and (b) shows the spatial distributions of the fields $E_x(x, y, z, t_n)$ for the CPW and slotline, respectively. These spatial distributions are sampled just below the

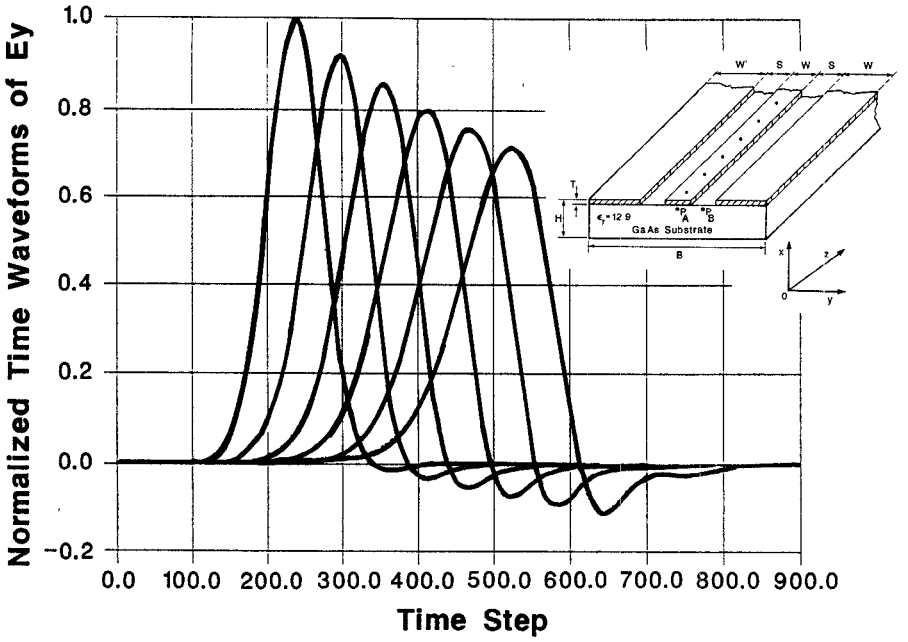

(a)

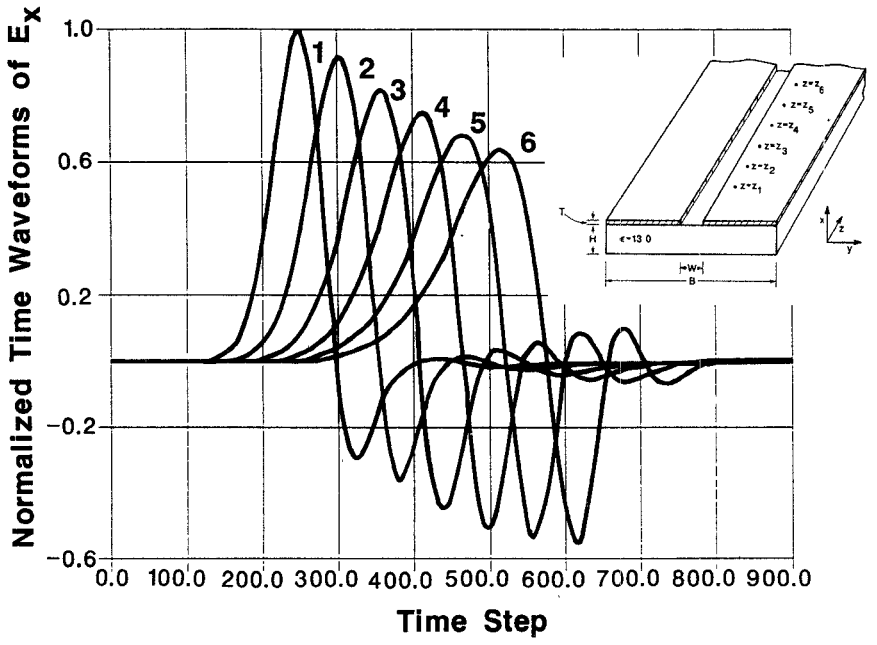

(b)

Fig. 3. (a) Normalized time waveforms of E_y for the CPW (case 1) at different z's. These signals are sampled just below the air–dielectric interface with a separation of ten spatial steps. The configuration of the CPW is also shown in the figure. Point P_A is the point at which the comparison in the Fig. 7(a) and (b) are made. (b) Normalized time waveforms of E_x for the slotline at different z's. These signals are sampled below the air–dielectric interface with a separation of ten spatial steps.

strips, i.e., just below the air–dielectric interface. The edge effect is apparent from an inspection of Fig. 2.

Instead of taking "snapshots" of the field waveforms, we can record the field at an arbitrary point $P(\xi_0, \zeta_0, \eta_0)$ in the computation domain. Fig. 3(a) shows the E_y components for the CPW. These curves are sampled at different z's ($z = idh$, $i = 20, 30, 40, 50, 60, 70$) just below the center strip. Fig. 3(b) contains similar curves for the slotline. These waveforms are sampled at points along the line with a separation of 10 spatial steps. The location of the sampled points for the slotline is shown in the same figure. As illustrated in the Fig. 3(a) and (b), the amplitude of the pulse decreases and its width increases as the pulse propagates along the line, due to radiation and dispersion effects.

C. Surface Current Distribution

In contrast to the spectral-domain analysis, the TD–FD method does not require an assumed surface current distribution on the metal strips. This distribution is obtained

directly from the tangential magnetic field. Fig. 4(a) and (b) shows the surface current $I(y, z_0, t_n)$ for the CPW and the slotline at different time steps (z_0 is fixed). It is also noted that, for the CPW, the current density distribution on the center strip reaches a maximum at the edges and a minimum at the center. On the side strips, the current density decays toward the outer edges. This rate of decay is helpful in determining the size of the enclosure for the CPW. It is observed that the longitudinal current density at the outer edge of the side strip is negligible when $W'/W > 8$ for a CPW with a substrate thickness $H = 0.52$ mm.

As can be seen from Fig. 4(b), the current density on the slotline reaches a maximum at the inner edge of the strip, and monotonically decreases toward the outer edges. The currents at the outer edges are also negligible for $B/W > 15$ with a substrate thickness $H = 0.1$ mm.

D. Dispersion Relations

As previously discussed, the dispersion relations can be found using (17) or (21). Comparisons of the effective dielectric constant $\epsilon_{\text{eff}}(f)$ for the CPW (case 1) are shown in Fig. 5(a). The result of present calculations (curve 1) agrees well with that of the empirical formula obtained by the spectral-domain analysis [2] (curve *2*) up to 120 GHz. The five points shown in Fig. 5(a), which are experimental data obtained by pulse (harmonic-mixing) electro-optic probing techniques [10], are also in good agreement with those numerical results in the range from 4.11 to 20.1 GHz. Fig. 5(b) shows a similar plot for the CPW (case 2), where curve *1* is the present result, curve *2* is from [2], and curve *3* is the theoretical result from [11]. As can be seen in Fig. 5(b), the first two results are in good agreement up to 17 GHz. The effective dielectric constant in [11], which is curve *3*, is slightly smaller than the other two results represented by curves *1* and *2*.

The dispersion relation for the effective dielectric constant of the slotline is shown in Fig. 5(c), where curve *1* is the simulated result from this calculation and curve *2* is from [12]. As indicated in this figure, the differences between the results are negligible except for the regions below 40 GHz and above 350 GHz. It should be pointed out that the formula for the effective dielectric constant in [12] is valid only for $0.01 \leqslant H/\lambda \leqslant H/\lambda_0$, where $\lambda_0 = 4.0H\sqrt{\epsilon_r - 1}$ is the cutoff wavelength of a TE_{10} mode. For the geometry under study, the formula is valid for the range 30 GHz $< f <$ 216 GHz. The upper limit of this range is due to the appearance of the high-order mode where the slotline is no longer in single-mode operation.

E. Frequency-Dependent Characteristic Impedance

The frequency-dependent characteristic impedance is found using either formula (18) or (22). The simulated impedances at dc are close to those obtained by the quasi-static analysis for both the CPW and slotline. Fig. 6(a) and 6(b) shows the complex impedances for the CPW cases 1 and 2, respectively. The real part of the impedance

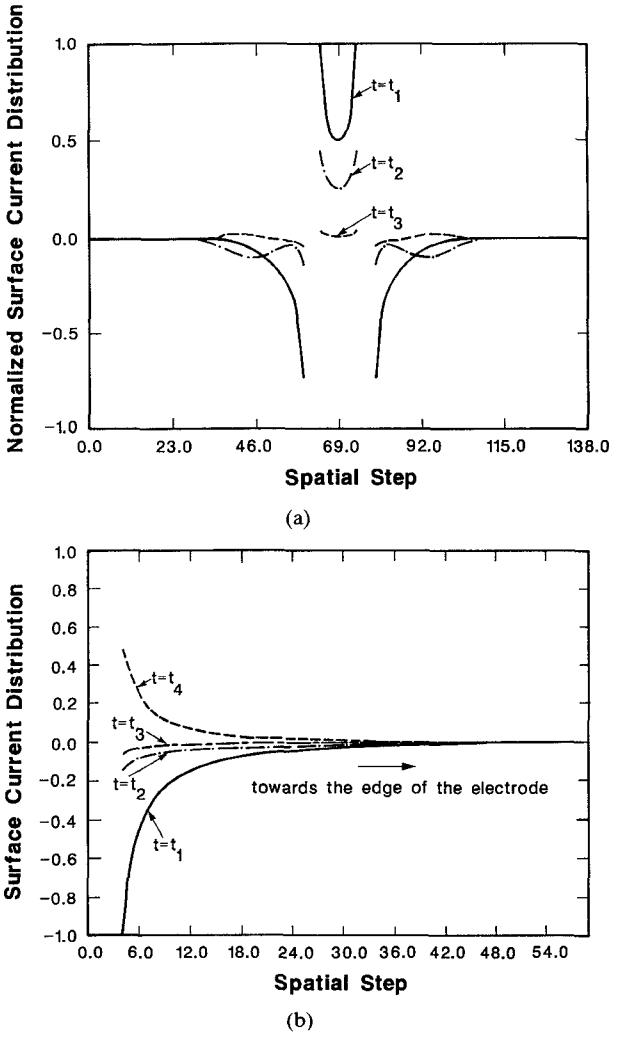

Fig. 4. (a) Surface current distributions for the CPW (case 1) at different time steps t_n. (b) Surface current distributions for the slotline at different time steps t_n. The current is monotonically decaying toward the edges.

is quite flat up to 150 GHz for case 1. In those plots, Z_r and Z_i are the real and imaginary parts of the complex impedance. Z_0 in Fig. 6(b) is the real impedance from [11].

The complex characteristic impedance for the slotline is shown in Fig. 6(c), where curve *1* is the present result of the real part of the impedance, and curve *2* is the real part of the impedance from the empirical formula in [12]. These two curves are quite close to each other. Curve *3* is the imaginary part of the impedance from the current calculation.

The imaginary part the characteristic impedance is due to radiation. This radiated power is carried partly by "space waves" and partly by the "surface waves." The reason why radiation affects the impedance can be explained from the circuit model definition of the characteristic impedance:

$$Z_0 = \sqrt{\frac{Z}{Y}} = \sqrt{\frac{R + j\omega L}{G + j\omega C}} \tag{23}$$

where Z is a distributed series impedance per unit length

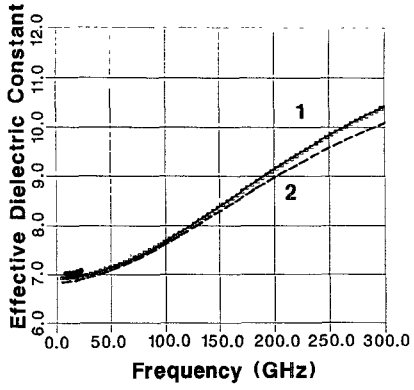

(a)

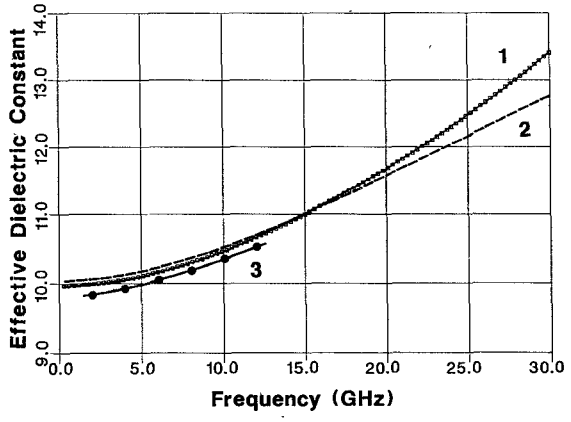

(b)

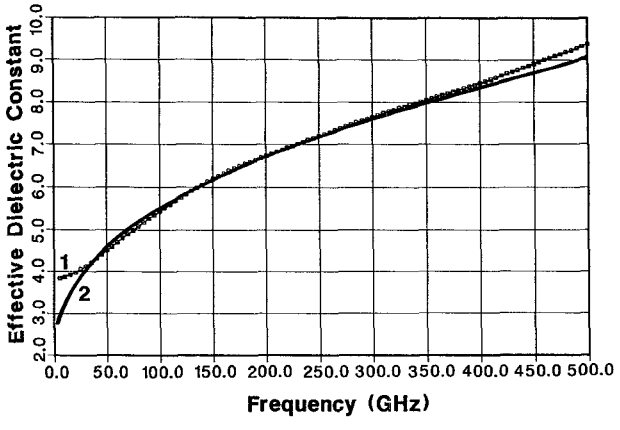

(c)

Fig. 5. (a) Comparisons of the effective dielectric constant for the CPW (case 1), where curve *1* is the present result, curve *2* is from [2], and the five points at low frequency are experimental data [10]. (b) Comparisons of the calculated result of the effective constant for CPW (case 2). Curve *1* is the present result, curve *2* is from [2], and curve *3* is the theoretical data from [11]. (c) Comparisons of the effective dielectric constants for slotline. Curve *1* is the present result and curve *2* is from [12].

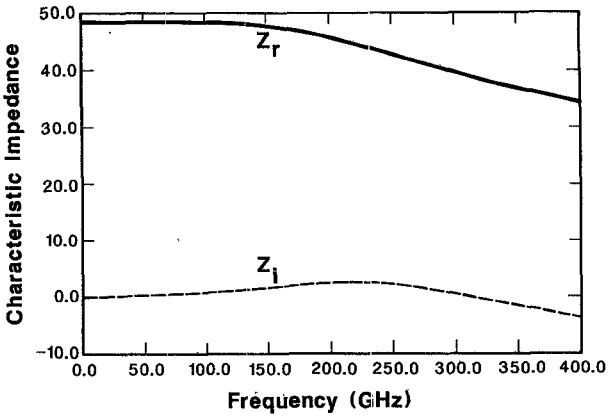

(a)

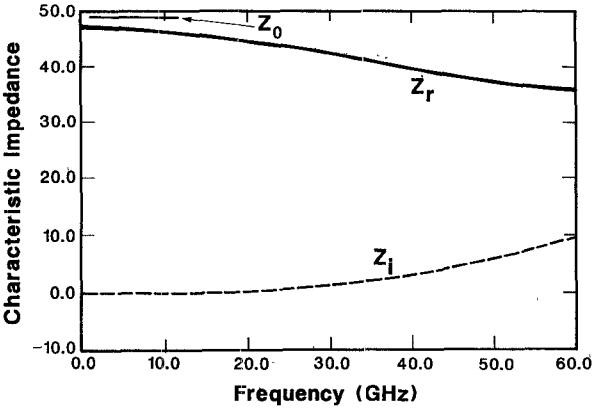

(b)

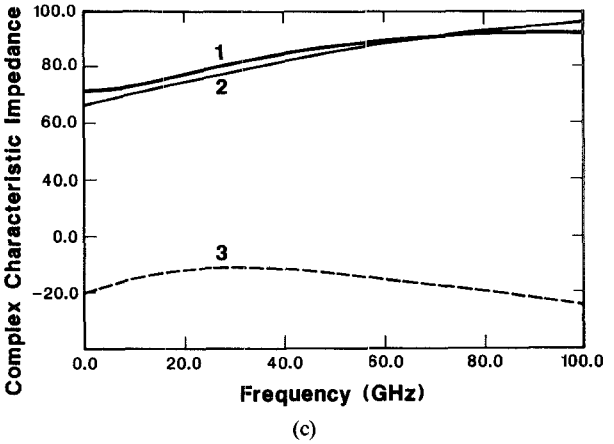

(c)

Fig. 6. (a) Complex characteristic impedance for the CPW (case 1). Z_r and Z_i are the real and imaginary parts of the impedance, respectively. (b) Complex characteristic impedance for the CPW (case 2). Z_r and Z_i are the real and imaginary parts of the impedance. Z_0 is the real characteristic impedance from [11]. (c) Complex characteristic impedance for the slotline. Curve *1* is the calculated result of the real part of the impedance, curve *2* is the real part of the impedance from the empirical formula in [12], and curve *3* is the imaginary part of the impedance from the current calculation.

and Y is a distributed shunt admittance per unit length. If the series distributed resistance R and shunt conductance G are not equal to zero, the characteristic impedance Z_0 will be complex. For many important problems, including the present one, the losses are finite but relatively small. If $R/\omega L \ll 1$ and $G/\omega C \ll 1$, the approximate expression for the characteristic impedance can be obtained from the binomial expression of (23). Here, we retain only first- and second-order terms:

$$Z_0 \approx \sqrt{\frac{L}{C}}\left[\left(1+\frac{R^2}{2\omega^2L^2}-\frac{3G^2}{8\omega^2C^2}+\frac{RG}{4\omega^2LC}\right)+j\left(\frac{G}{2\omega C}-\frac{R}{2\omega L}\right)\right] \quad (24)$$

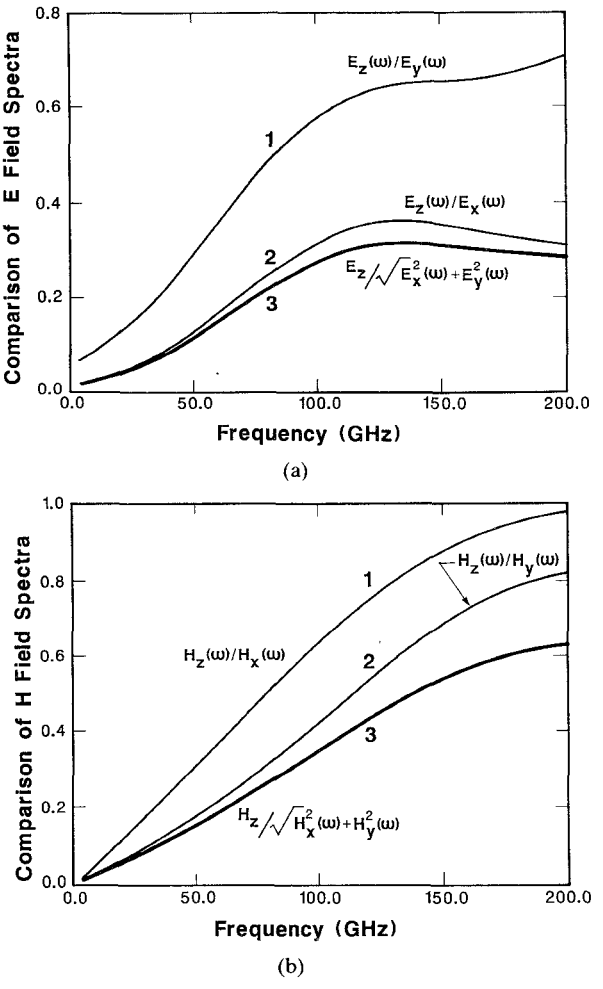

Fig. 7. (a) Comparisons of the Fourier transforms of the electric field components for the CPW (case 1) at P_A. Curves *1*, *2*, and *3* are the ratios $E_z(\omega)/E_y(\omega)$, $E_z(\omega)/E_x(\omega)$, and $E_z(\omega)/\sqrt{E_x^2(\omega)+E_y^2(\omega)}$, respectively. (b) Comparisons of the Fourier transforms of the magnetic field components for the CPW (case 1) at P_A. Curves *1*, *2*, and *3* are the ratios $H_z(\omega)/H_x(\omega)$, $H_z(\omega)/H_y(\omega)$, and $H_z(\omega)/\sqrt{H_x^2(\omega)+H_y^2(\omega)}$, respectively.

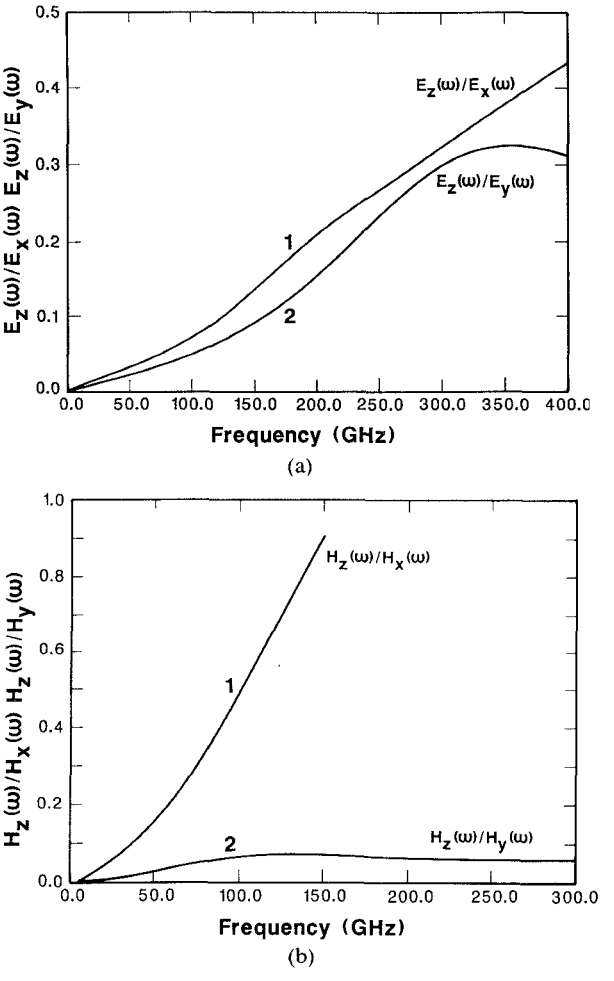

Fig. 8. (a) Comparisons of the Fourier transforms of the electric field components for the slotline. Curves *1* is the ratio $E_z(\omega)/E_x(\omega)$; curve *2* is the ratio $E_z(\omega)/E_y(\omega)$. The comparison is made at the median plane of the substrate beneath the point $z = z_4$ shown in Fig. 3(b). (b) Comparisons of the Fourier transforms of the magnetic field components for the slotline. Curves *1* is the ratio $H_z(\omega)/H_x(\omega)$; curve *2* is the ratio $H_z(\omega)/H_y(\omega)$. The comparison is made at the median plane of the substrate beneath the point $z = z_4$ shown in Fig. 3(b).

where L, C, R, and G are all frequency dependent. It is interesting to note from both Fig. 6(a) and (b) that the impedance is real at low frequencies, but as the frequency increases, it becomes complex. At a high frequency, the impedance becomes real again as a result of transverse resonance which happens at $G/C = R/L$.

F. Transverse Versus Longitudinal Fields

Although the coplanar waveguide and slotline are essentially surface-oriented planar transmission lines, quasi-TEM mode analysis is still useful for low-frequency applications. But at what frequency does the quasi-TEM model break down?

We have compared E field components at point P_A. The location of the point P_A is just below the center strip as shown in Fig. 3(a). It is observed that the peak value ratios of E_x: E_y: E_z are 1.00:0.28:0.025. Similarly, the peak value ratios of the magnetic field H_x: H_y: H_z are 0.400:1.00:0.16. From the above two comparisons, we have a rough idea of the amplitude of the longitudinal components. By taking Fourier transforms of these components, we can compare these field components in the frequency domain. Fig. 7(a) and (b) shows the ratios of the longitudinal components to the transverse components. In Fig. 7(a), curves *1*, *2*, and *3* are the ratios $E_z(\omega)/E_y(\omega)$, $E_z(\omega)/E_x(\omega)$, and $E_z(\omega)/\sqrt{E_x^2(\omega)+E_y^2(\omega)}$, respectively. As indicated in Fig. 7(a), $E_z(\omega)/\sqrt{E_x^2(\omega)+E_y^2(\omega)}$ is 0.12 at 50 GHz. Fig. 7(b) shows the corresponding curve for the magnetic field (CPW case 1). Ratios $H_z(\omega)/H_x(\omega)$, $H_z(\omega)/H_y(\omega)$, and $H_z(\omega)/\sqrt{H_x^2(\omega)+H_y^2(\omega)}$ are shown in curves *1*, *2*, and *3*, respectively. $H_z(\omega)/\sqrt{H_x^2(\omega)+H_y^2(\omega)}$ is 0.15 at 50 GHz. The above results vary with the points at which these ratios are evaluated.

From the previous discussion, we know that the longitudinal components, especially the $\vec{H}$ field, increase with increasing frequency. At a high enough frequency, an elliptically polarized magnetic field will appear in the

slots at the air–dielectric interface. If one allows longitudinal fields to be 10–20 percent of the transverse fields at the point P_4 for the CPW in Fig. 3(a), the operating frequency can go up to 50 GHz for the present structure ($W = 135\ \mu$m, $S = 65\ \mu$m, $H = 500\ \mu$m).

It is believed that the mode on the slotline is almost a transverse electric mode. This can also be examined by evaluating $H_z(\omega)$ and $E_z(\omega)$. Comparisons of the Fourier transforms of these electric and magnetic fields are shown in Fig 8(a) and (b). These comparisons are made at the median plane of the substrate beneath the point $z = z_4$ (see Fig. 3(b)). It is observed from Fig. 8(a) and (b) that up to 120 GHz, the longitudinal electric component is less than 10 percent of the transverse component, while $H_z(\omega)/H_x(\omega)$ exceeds 0.1 above 60 GHz. As mentioned before, the voltage is not uniquely defined since there are nonzero values of E_z and H_z, especially at high frequencies. Equation (18) breaks down if the longitudinal components are not negligible. Again, the above discussion varies with the points at which the comparisons are made.

VII. Summary and Conclusion

The coplanar waveguide and slotline have been analyzed by the time-domain finite-difference method. The basic principles and procedures have been discussed, along with some specific problems in the implementation. Time- and frequency-domain results have been presented and explained. The frequency results, such as the effective dielectric constant and the characteristic impedance, agree well with spectral domain data over a wide frequency range. The effective dielectric constants for the CPW (case 1) are also in good agreement with the experimental data up to 20 GHz. The validity of the quasi-static analysis has been checked.

References

[1] J. B. Knorr and K. D. Kuchler "Analysis of coupled slots and coplanar strips on dielectric substrate," *IEEE Trans. Microwave Theory Tech.*, vol. MTT-23, pp. 541–548, July 1975.

[2] G. Hasnain, A. Dienes, and J. R. Whinnery, "Dispersion of picosecond pulses in coplanar transmission lines," *IEEE Trans. Microwave Theory Tech.*, vol. MTT-34, pp. 378–741, June 1986.

[3] T. Itoh and R. Mittra, "Dispersion characteristics of slotlines," *Electron Lett.*, vol. 7, pp. 364–365, July 1971.

[4] X. Zhang, J. Fang, K. K. Mei, and Y. Liu "Calculation of the dispersion characteristics of microstrips by the time-domain finite-difference method," *IEEE Trans. Microwave Theory Tech.*, vol. 36, pp. 263–267, Feb. 1988.

[5] G. C. Liang, Y. W. Liu, K. K. Mei, "On the characteristic of the slot line," in *1989 IEEE AP-S Int. Symp. Dig.* June 1989, pp. 718–721.

[6] G. C. Liang, Y. W. Liu, K. K. Mei, "Analysis of coplanar waveguide by the time-domain finite-difference method," in *1989 IEEE MTT-S Int. Microwave Symp. Dig.*, June 1989, pp. 1005–1008.

[7] G. Mur, "Absorbing boundary conditions for finite-difference approximation of the time-domain electromagnetic field equations," *IEEE Trans. Electromagn. Compat.*, vol. EMC-23, pp. 1073–1077, Nov. 1981.

[8] K. S. Yee, "Numerical Solution of initial boundary value problems involving Maxwell's equations in isotropic media," *IEEE Trans. Antennas Propagat.*, vol. AP-14, pp. 302–307, May 1966.

[9] J. Fang and K. K. Mei, "A super-absorbing boundary algorithm for solving electromagnetic problems by time-domain finite-difference method," in *1988 IEEE AP-S Int. Symp. Dig.*, June 1988, pp. 472–475.

[10] Z. H. Zhu, *et al.*, "Measurements on standing waves in GaAs coplanar waveguide at frequencies up to 20.1 GHz by electro-optic probing," *J. Appl. Phys.*, vol. 64, pp. 419–421, July 1988.

[11] T. Kitazawa, Y. Hayashi, and M. Suzuki, "A coplanar waveguide with the metal-coating," *IEEE Trans. Microwave Theory Tech.*, vol. MTT-24, pp. 604–608, Sept. 1976.

[12] R. Garg and K. C. Gupta, "Expressions for wavelength and impedance of a slotline," *IEEE Trans. Microwave Theory Tech.*, vol. MTT-24, p. 523, Aug. 1976.

Guo-chun Liang (S'86) was born in Jiangsu, China, on October 14, 1959. He received the B.S. degree in electrical engineering from the East China Institute of Technology, Naijing, China, in 1982, and the M.S. degree in electrical engineering from the University of Electronics Science and Technology of China (UEST), Chengdu, China, in 1985.

In 1985 and 1986, he worked in the Microwave Center at UEST. Currently, he is a research assistant in the Department of Electrical Engineering and Computer Sciences at the University of California at Berkeley, where he is working toward the Ph.D. degree. His research interests include superconductive integrated circuits, electromagnetics of superconductors, and modeling of microwave monolithic integrated circuit components.

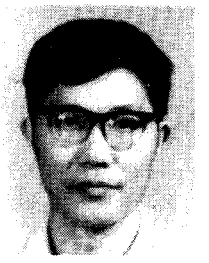

Yao-wu Liu was born in Chongqing, China, on November 28, 1943. He graduated and received the M.S. and Ph.D. degrees from the University of Electronic Science and Technology of China, Chengdu, China, in 1967, 1981, and 1984, respectively.

From 1970 to 1978, he worked as an assistant engineer in microwave communications in Sichuan, China. In 1986, he became an associate professor at the University of Electronic Science and Technology of China. He was a visiting scholar with the Department of Electrical Engineering at the University of Utah from April to November of 1986. Since December of 1986, he has been a visiting scholar with the Department of Electrical Engineering and Computer Sciences of the University of California at Berkeley. His general research interests include numerical procedures of finite element and finite difference methods for passive microwave components, electromagnetic scattering, electromagnetic biological effects, the design and measurement of passive and active microwave circuits, and special antennas.

Kenneth K. Mei (S'61–M'63–SM'76–F'79) received the B.S.E.E., M.S., and Ph.D. degrees in electrical engineering from the University of Wisconsin, Madison, in 1959, 1960, and 1962, respectively.

He became a member of the faculty of the Department of Electrical Engineering and Computer Sciences of the University of California at Berkeley in 1962. He is now a Professor there. His main areas of interest are antennas, scattering, and numerical methods in solving electromagnetic problems.

Dr. Mei received the best paper award and honorable mention of the best paper award in 1967 and 1975, respectively, form the IEEE Antennas and Propagation Society. He is a member of URSI/USNC. He served as a member of AdCom of the IEEE Antennas and Propagation Society and as an Associate Editor of its Transactions.